



OPEN

Nearly-freestanding supramolecular assembly with tunable structural properties

Tommaso Caruso^{1,2,12}, Oreste De Luca^{2,3,12}, Nicola Melfi¹, Alfonso Policicchio^{1,2}, Michele Pisarra^{4,5,6}, Nicolas Godbert^{7,8}, Iolinda Aiello^{7,8,9}, Eugenia Giorno^{7,8}, Daniela Pacilè¹, Paolo Moras¹⁰, Fernando Martín^{5,6,11}, Petra Rudolf³, Raffaele Giuseppe Agostino^{1,2} & Marco Papagno^{1,2}✉

The synthesis and design of two-dimensional supramolecular assemblies with specific functionalities is one of the principal goals of the emerging field of molecule-based electronics, which is relevant for many technological applications. Although a large number of molecular assemblies have been already investigated, engineering uniform and highly ordered two-dimensional molecular assemblies is still a challenge. Here we report on a novel approach to prepare wide highly crystalline molecular assemblies with tunable structural properties. We make use of the high-reactivity of the carboxylic acid functional moiety and of the predictable structural features of non-polar alkane chains to synthesize 2D supramolecular assemblies of 4-(decyloxy)benzoic acid (4DBA; $C_{17}H_{26}O_3$) on a Au(111) surface. By means of scanning tunneling microscopy, density functional theory calculations and photoemission spectroscopy, we demonstrate that these molecules form a self-limited highly ordered and defect-free two-dimensional single-layer film of micrometer-size, which exhibits a nearly-freestanding character. We prove that by changing the length of the alkoxy chain it is possible to modify in a controlled way the molecular density of the “floating” overlayer without affecting the molecular assembly. This system is especially suitable for engineering molecular assemblies because it represents one of the few 2D molecular arrays with specific functionality where the structural properties can be tuned in a controlled way, while preserving the molecular pattern.

Complex molecular architectures are usually constructed by connecting molecular building blocks through non-covalent bonding, allowing for a variety of different supramolecular structures and phases to emerge^{1–6}. When solid surfaces are used as supports, the molecular self-assembly can be regarded as a two-dimensional (2D) process, and the structural and electronic properties, such as molecular packing, the number and typologies of domains, and the binding energy of the molecular levels, strongly depend on the interplay between the intermolecular forces and the interaction between the adsorbate and the underlying support^{7–9}.

A suitable choice of molecular building blocks and supporting substrates would enable, in principle, synthesizing and designing 2D supramolecular assemblies with specific functionalities, disclosing exciting new opportunities in many areas of science and technology^{10–13}. Key steps to these accomplishments are (a) to understand how molecules self-arrange, and (b) to master the growth of homogeneous, highly ordered and defect-free films with tunable properties^{14,15}.

¹Dipartimento di Fisica, Università della Calabria, 87036 Rende (Cs), Italy. ²Laboratorio di Spettroscopia Avanzata dei Materiali, STAR IR, Via Tito Flavio, Università della Calabria, 87036 Rende (CS), Italy. ³Zernike Institute for Advanced Materials, University of Groningen, 9747 AG Groningen, The Netherlands. ⁴INFN, Sezione LNF, Gruppo Collegato di Cosenza, Cubo 31C, 87036 Rende (CS), Italy. ⁵Instituto IMDEA Nanociencia, Calle Faraday 9, 28049 Madrid, Spain. ⁶Departamento de Química, Universidad Autónoma de Madrid, Módulo 13, 28049 Madrid, Spain. ⁷MAT_InLAB (Laboratorio di Materiali Molecolari Inorganici), Centro di Eccellenza CEMIF.CAL, LASCAMM CR-INSTM, Unità INSTM della Calabria, Dipartimento di Chimica e Tecnologie Chimiche, Università della Calabria, 87036 Rende (CS), Italy. ⁸LPM-Laboratorio Preparazione Materiali, STAR-Lab, Università della Calabria, Via Tito Flavio, 28049 Rende (CS), Italy. ⁹CNR-Nanotec, UoS di Cosenza, Dipartimento di Fisica, Università della Calabria, 87036 Rende (CS), Italy. ¹⁰Istituto di Struttura della Materia-CNR (ISM-CNR), 34149 Trieste, Italy. ¹¹Condensed Matter Physics Center (IFIMAC), Cantoblanco 28049, Madrid, Spain. ¹²These authors contributed equally: Tommaso Caruso and Oreste De Luca. ✉email: marco.papagno@fis.unical.it

Small carboxylated molecules present an ideal testing playground for exploring and establishing strategies to design novel molecular assemblies. Owing to their functional groups, these molecules can bind to one another through strong and directional hydrogen bonding. Supported on solid surfaces, these molecular building blocks can self-assemble through electrostatic or van der Waals interaction to form complex 2D architectures^{1–6,13,16–28}.

Although hundreds of structures have been realized so far, predicting and designing 2D crystalline materials are still difficult tasks. One remarkable exception are alkyls, which form self-assembled monolayers that can be modulated by varying the chain length^{29–32}. In these assemblies the molecules adopt a lamellar structure where the alkyl chains pack side-by-side flat on the surfaces. The specific structure depends on the number of the carbon atoms in the alkyl chain through a mechanism known as “odd-even” effect: Alcohols with an even (odd) number of carbons interact weakly (strongly) with the substrate producing a nearly tilted (orthogonal) alcohol orientation with respect to the lamellae.

The present study takes advantage of the high-reactivity of the carboxylic acid functional moiety and of the predictable structural features of non-polar alkane chains to synthesize nearly-free standing 2D supramolecular assemblies of 4-(decyloxy)benzoic acid (4DBA; $C_{17}H_{26}O_3$) on a Au(111) surface with tunable structural properties. Scanning tunneling microscopy reveals that the self-assembly is self-limited, yielding a highly ordered and defect-free single-layer film of 4DBA molecules with uniform micrometer-sized grains on the noble metal surface. We provide evidence that by varying the length of the alkoxy group it is possible to modify the molecular density without affecting the molecular arrangement, and therefore to tune in a controlled way the structural properties of the supramolecular assembly. By combining high-resolution scanning tunneling microscopy, theoretical modeling and photoemission spectroscopy, we investigated the molecular arrangement on the Au(111) surface and demonstrated the nearly-freestanding character of the 4DBA supramolecular assembly.

Results and discussion

The 4DBA molecule, sketched in Fig. 1a, is a substituted benzoic acid with a C_{10} alkoxy chain. On the Au(111) surface, the growth of these molecules is self-limited to a single-layer film. A representative scanning tunneling microscopy (STM) image of a 4DBA monolayer on Au(111) is presented in Fig. 1b. On this large scale image, the molecular assembly is visualized as a set of bright parallel stripes on a darker imaged substrate. The assembly covers the wide and atomically flat terraces of the metallic surface, displaying a uniform, defect-free and highly ordered pattern over the whole sample surface investigated by STM (surface area $\sim 10 \mu\text{m}^2$). In most cases, the molecular stripes display a perfect alignment between the adjacent wide terraces of the metallic substrate, as shown in the magnified view presented in Fig. 1c. Different orientations of the molecular stripes are however observed in those sample regions characterized by several step edges (see left-hand side of Fig. 1b and Fig. S1 of the Supplementary Information).

Scanning tunneling microscopy shows streaks or no image at all for an incomplete single-layer film at all temperatures accessible in our experiment ($T > 160 \text{ K}$), indicating that the 4DBA molecules are too mobile for imaging. This behavior is distinctive of weakly interacting overlayers^{33,34}.

In Fig. 1d (and Fig. S2a) we present a STM image of the same sample surface collected with a different bias voltage. Here, beneath the molecular network, the Au herringbone reconstruction is also seen as bright lines in the STM image^{35–38}. This indicates that the adsorbed layer does not substantially change the surface stress of the substrate at odd with molecular overlayers that chemisorb strongly^{37–43}. Furthermore, we note that the orientation of the molecules do not change on the different sides of the elbow position of the herringbone reconstruction (see Fig. S2b of the Supplementary Information). Both results are distinctive of a weakly interacting overlayer.

High-resolution STM images of single-layer 4DBA unveil the details of the internal molecular structure, orientation, and packing of the ordered adlayer. We found two distinct molecular arrangements, presented in Fig. 2a,c, which both produce stripes on a larger scale. Each molecule is visualized here as a bright spot with a fainter tail; We associate the former to the carboxylic acid group and the latter to the alkoxy chain. Groups of molecules are separated by darker regions (lamellae). Similar molecular arrangements have been observed for monocarboxylic

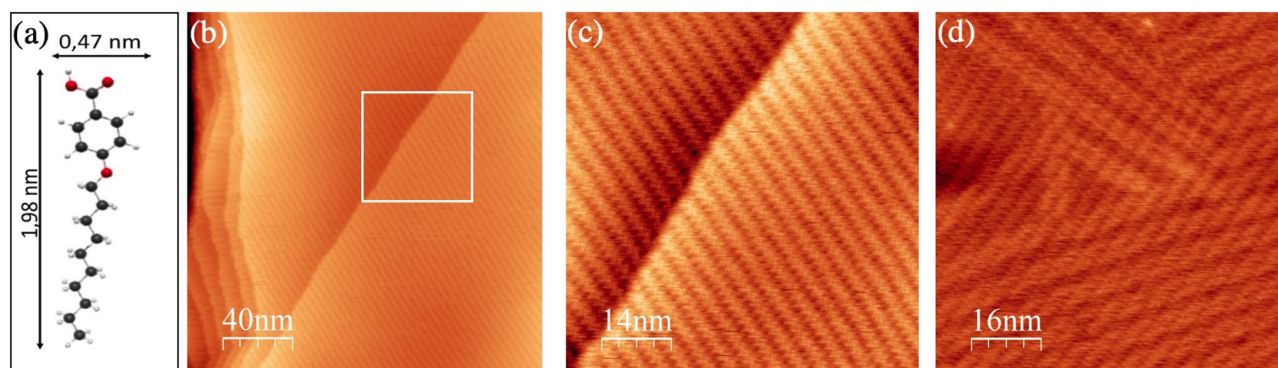


Figure 1. (a) Sketch of the 4DBA molecule (carbon atoms are drawn in dark grey, oxygen atoms in red and hydrogen atoms in white). Large scale (b) and close-up (c) STM images of the molecular assembly of 4DBA on Au(111) ($V_b=1.6 \text{ V}$; $I_t=100 \text{ pA}$; $T=300 \text{ K}$); (c) Represents area marked by the white box (b). (d) Constant-current STM image of 4DBA/Au(111) ($V_b=1.3 \text{ V}$; $I_t=100 \text{ pA}$; $T=300 \text{ K}$) displaying both the supramolecular pattern and the herringbone reconstruction.

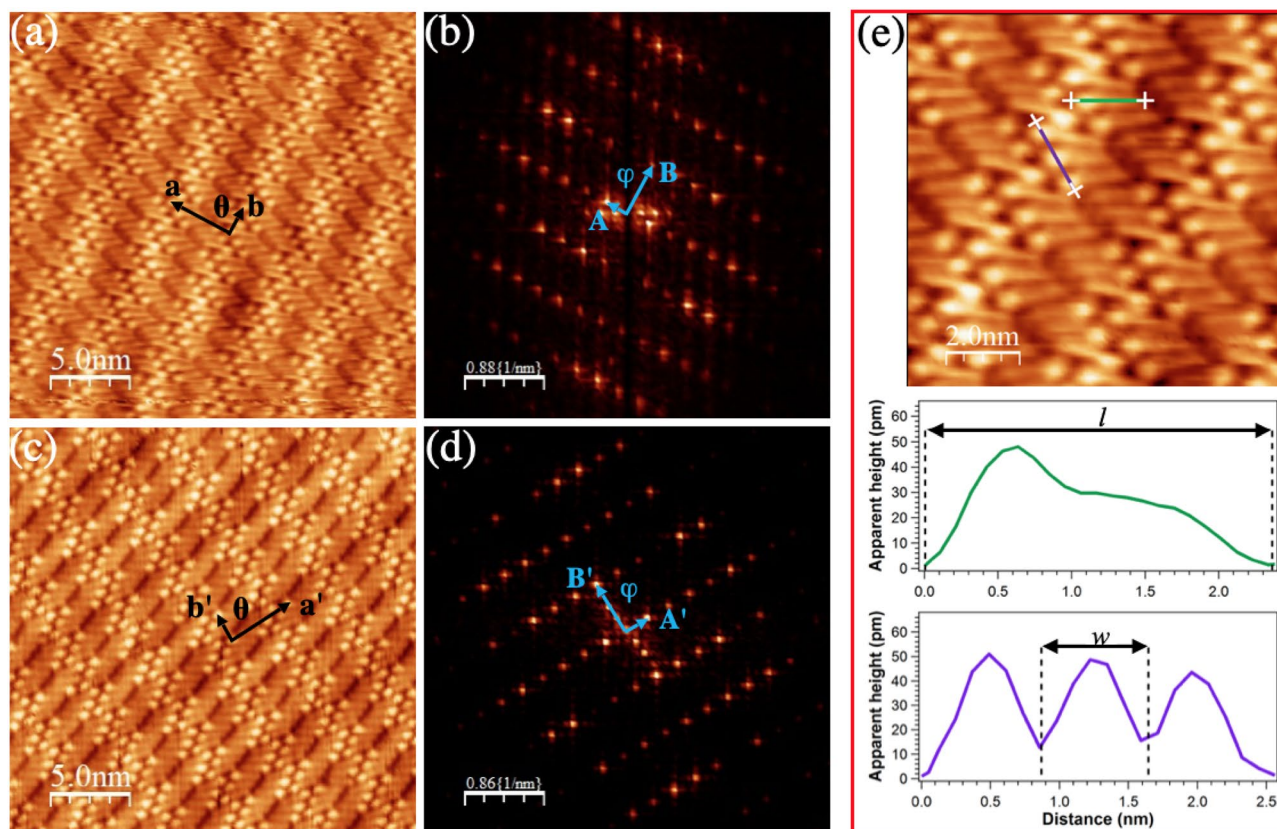


Figure 2. (a,c) Constant-current STM images ($V_b=1.1$ V; $I_t=100$ pA; $T=300$ K) displaying two different supramolecular assemblies observed for 4DBA/Au(111); The black arrows represent the unit cell vectors. (b) and (d) are the Fourier transforms of panels (a) and (c), respectively; The blue arrows identify the unit cell vectors in the reciprocal space. (e) Top panel: STM image of 4DBA/Au(111) ($V_b=1.1$ V; $I_t=100$ pA; $T=300$ K); Bottom panel: line profiles along the green and blue lines of the top panel marking the length (l) and benzoic head width (w) of the 4DBA molecule.

acids deposited on HOPG^{21,28}. The Fourier analysis of Fig. 2a,c, displayed in Fig. 2b,d, respectively, proves that, though the arrangements are not equivalent, they share the same unit cell ($\mathbf{a} = 3.9 \pm 0.2$ nm, $\mathbf{b} = 1.7 \pm 0.1$ nm, $\Theta = 91.5^\circ \pm \epsilon$). The unit cell contains 6 molecules and corresponds to a molecular density $\rho_{4DBA} = 0.89$ nm⁻².

The line profiles parallel and perpendicular to the molecular axis presented in Fig. 2e provide an estimate of the length ($l = 1.9 \pm 0.1$ nm) and benzoic head width ($w = 0.5 \pm 0.1$ nm) of the 4DBA molecule, in excellent agreement with the predicted ones⁴⁴, and strongly suggests a parallel adsorption geometry on the metallic surface. This finding is consistent with the planar geometry adopted by monocarboxylic acids on HOPG^{21,28}, and by similar molecules like for example benzoic, trimesic or isophthalic acid on Au(111)^{20,25,27,32,45}, HOPG^{11,29,31}, and benzene on face-centered cubic {111} noble metal surfaces^{7,8,46–50}.

STM investigations on alkyl molecules adsorbed on Au(111)³² and HOPG^{11,17,19,21,28,29,31} revealed different 2D molecular patterns depending on the parity (even or odd) of the carbon count in the alkyl chain. Inspired by these results, we explored the possibility to modulate the periodicity of the assembly by changing the alkoxy chain length but always keeping an even number of the carbon atoms.

Figure 3a,b shows the STM images collected on the Au(111) surface covered by a single-layer of 4TBA (4-(tetradecyloxy)benzoic acid; C₂₁H₃₄O₃) and 4HBA (4-(hexyloxy)benzoic acid; C₁₃H₁₈O₃). The former has four more carbon atoms in the chain than 4DBA, while the latter has four less. Collecting STM data on the shorter 4HBA was quite difficult, most likely because of the lower adsorption energy, which reduces the stability of the assembly and hence affects the quality of the image. Both supramolecular assemblies display the same molecular arrangement found for the 4DBA but the unit cells are different ($\mathbf{a} = 3.9 \pm 0.2$ nm, $\mathbf{b} = 1.8 \pm 0.1$ nm, $\Theta = 93.0^\circ \pm 1.2^\circ$ for the 4TBA; $\mathbf{a} = 3.6 \pm 0.2$ nm, $\mathbf{b} = 1.8 \pm 0.1$ nm, $\Theta = 75.0^\circ \pm 1.2^\circ$ for 4HBA), as well as the molecular density, which is $\sim 10\%$ higher for the 4HBA than for the 4TBA overlayer.

The 4DBA/Au(111) system therefore represents one of the few supramolecular surface assemblies that allows, through a proper choice of the length of the alkoxy chain, to modulate the structural properties of the ensemble in a controlled way without altering the molecular arrangement.

To gain insight on the observed molecular structure, we investigated the 4DBA assembly by means of first principles atomistic calculations. Inspection of the frontier molecular orbitals (see Fig. S10 in the SI) of 4DBA, 4TBA, and 4HBA shows that the highest occupied molecular orbitals and lowest unoccupied molecular orbitals of these molecules have very similar energies and shapes, demonstrating that the alkyl tail acts as a buffer spacing medium capable of distancing the reactive zones of the molecule in the self-assembly.

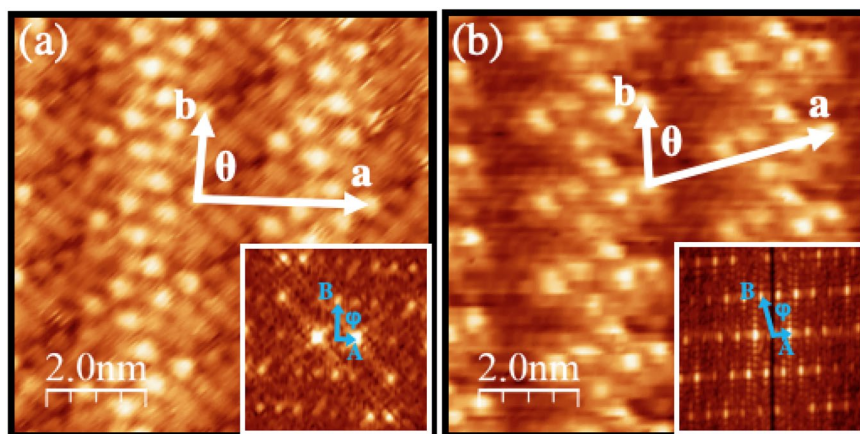


Figure 3. Constant-current STM images of (a) 4TBA/Au(111) ($V_b=0.22$ V; $I_t=160$ pA; $T=300$ K) and (b) 4HBA/Au(111) ($V_b=0.50$ V; $I_t=500$ pA; $T=300$ K). White vectors identify the unit cell vectors. The insets of panels (a) and (b) shows the corresponding Fourier transform; The blue vectors in the insets mark the unit cell vectors in the reciprocal space.

STM results suggest that the molecule-substrate interaction plays a minor role in dictating the molecule arrangement. Indeed, test calculations on a simplified system (see Supplementary Information section “2D self assemblies of 4DBA molecules”) show that the molecule-Au(111) interaction is of non-covalent nature. For these reasons, we have analyzed the stability of several self-standing 2D molecular arrangements of 4DBA.

Firstly, we note that, although the 4DBA is an achiral molecule, deposition of a self-assembly of 4DBA molecules on the metal surface can give rise to a surface-induced “supramolecular-chirality”. As shown in detail in section “2D self assemblies of 4DBA molecules” of the Supplementary Information, two equi-energetic 4DBA conformer exists, which only differ in the relative position of the H atom in the carboxylic group with respect to the orientation of the alkyl tail. The 2D self-assembly is realized by two 4DBA forming a dimer through a double hydrogen bond between the carboxylic groups. Such dimers then organize by means of inter-dimer interactions in 2D packed structures (see Fig. 4a,b). We focused on unit cells composed by either 1 or 3 dimers. Our calculations demonstrate that the 3-dimer unit cell arrangements (see Fig. 4a,b) result in a total energy ~ 0.2 eV/molecule lower than that of the 1-dimer unit cell systems. Since the hydrogen atom of the carboxylic functional group is probably free to transfer from one oxygen atom to the other in each molecule and, possibly, within a dimer pair of adsorbed molecules, the induced chirality derives from the orientation of the alkoxy chain grafted onto the benzene ring.

Our calculations reveal two equi-energetic 3-dimers arrangements. In both cases, the self-assembly unit cell is made of three 4DBA-dimers bonded by means of double hydrogen bonds (one of the three is highlighted by the green box in Fig. 4a,b) through the carboxylic acid groups with bond length ~ 2.1 Å. To minimize the steric repulsion, the alkoxy chains arrange themselves in a fully extended and planar configuration. Each dimer is weakly bonded to the neighboring dimer by weak lateral C-H \cdots O interactions^{51,52} (two of them are highlighted by blue boxes in Fig. 4a,b). In the minimum energy configuration, two 4DBA of the molecular building block, highlighted by red arrows in Fig. 4a,b, adopt an inverted conformation with respect to the others. We point out that this is a necessary condition to link adjacent building blocks by means of C-H \cdots O interactions (purple box in Fig. 4c,d) and to form a stable 2D system. In this way, the supramolecular assembly optimizes its configuration, minimizing the steric repulsion between the alkoxy chains while increasing the net number of C-H \cdots O interactions per molecule.

Interestingly, the unit cells of the two equi-energetic self-assemblies found in the calculations are mirror images, further demonstrating the surface-induced supramolecular chirality⁷. In Fig. 4e,f we overlay the results of our simulations with the STM images of the supramolecular assemblies to emphasize the excellent agreement between the minimum energy arrangement provided by the density functional theory calculations and the experimental STM images.

The electronic structure of 4DBA/Au(111) was investigated by photoemission spectroscopy. The measured spectrum of C 1s core level region, presented in Fig. 5a, displays a shape mirroring the presence of differently interacting C atoms. In particular, we observe a main peak at binding energy 284.0 eV and two minor components at 285.7 and 288.1 eV. Similar line-shapes have been recorded for the α -form of crystalline *para*-aminobenzoic acid⁵³, assemblies of isophthalic acid on Ag(111) and trimesic acids on Cu(111)²².

The simulated spectrum of the C 1s core level region of a single 4DBA in gas phase, presented in Fig. 5b, is in remarkable agreement with the experimental findings. We included in the inset of Fig. 5b a sketch of the 4DBA molecule with the C atoms marked by different colors. The binding energy of the 1s orbital of each C atom is marked by a colored bar on the horizontal axis of the plot. As expected, the C atoms of the COOH group have the highest binding energy, followed by the C atoms bonded to the O atom of the molecular tail. The remainder of the C atoms generates the main peak at the lowest binding energy. The valence band spectrum of clean Au(111), shown in Fig. 5c (gray dotted line), is dominated by the Au 5d states in the energy region in between 8 and 2 eV below the Fermi level (E_F). Close to E_F a feature due to the Shockley surface state is distinguished, in agreement

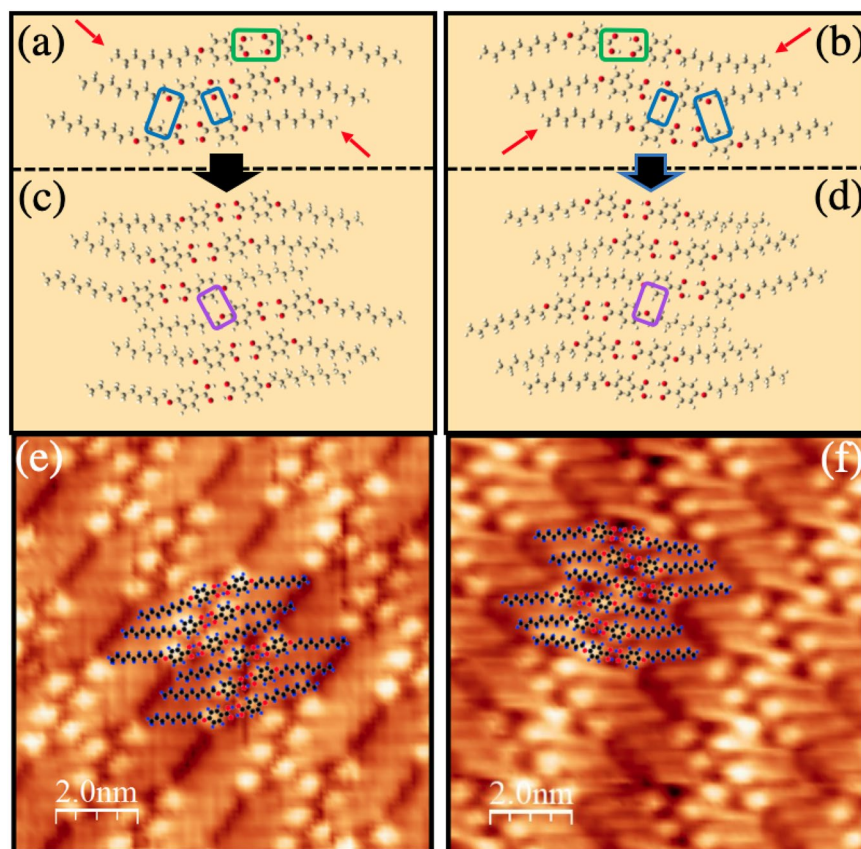


Figure 4. (a,b) Simulated 4DBA molecular building blocks having opposite supramolecular chirality. The red arrows mark the 4DBA molecules in a different conformation with respect to the others. The green box highlights the double hydrogen bonds within one dimer, whereas the blue boxes mark the electrostatic C–H \cdots O interaction between dimers. (c,d) The optimized supramolecular assemblies from the building blocks presented in panel (a) and (b), respectively. The purple box encloses the C–H \cdots O interaction between adjacent building blocks. (e,f) The optimized supramolecular structures of panels (c,d) are overlaid to the STM images of the two experimental assemblies ($V_b=1.1$ V; $I_t=100$ pA; $T=300$ K).

with previous results^{54,55}. After the synthesis of the 4DBA supramolecular assembly, the valence band spectrum (black curve in Fig. 5c) is clearly changed but the high intensity of the Au 5d levels prevents a clear identification of the occupied molecular orbitals. The surface state is still present below the supramolecular assembly but its spectral-weight intensity is smaller. This is better seen in the angle-resolved photoemission spectra of Fig. 5d,e presenting the Shockley state of bare Au(111) sample before and after the assembly of the 4DBA overlayer. On Au(111), the Shockley state displays a “parabolic-like” dispersion identical for all in-plane directions with a minimum at the $\bar{\Gamma}$ point^{56,57}. Similarly to the herringbone reconstruction, the Shockley state is quite sensitive to the strength of the interaction with the overlayer: For a strong interaction, a substantial shift of the energy minimum toward lower energies and a shorter life-time has been observed, up to a complete disappearance^{58–61}. In contrast, the sharpness of the Shockley state along with the unaltered energy minimum observed in Fig. 4f and Fig. S4 supports a negligible 4DBA–Au interaction, in agreement with the STM and DFT findings.

Conclusion

We characterized the structure and the electronic properties of the 4DBA supermolecular assembly and found that a highly-ordered, uniform and self-limiting defect-free single-layer film covering the whole Au(111) surface is formed. High-resolution STM measurements combined with DFT calculations revealed that the 4DBA molecules self-assemble and interact via a combination of hydrogen bonds and lateral weak C–H \cdots O interactions to form a stable molecular 2D network. We prove that by varying the alkoxy chain length of the molecule it is possible to tune the molecular density of the overlayer without affecting the way the molecules arrange. The measured electronic structure supports a nearly-freestanding character of the supramolecular assembly, in agreement with STM and DFT findings. Since an alkoxy chain linked to a molecule with a functional group is the prerequisite for this type of assemblies, systems other than 4DBA should exhibit the same behavior. We therefore believe this work may represent an important step toward engineering molecular devices using supramolecular principles, mostly because the “floating” character of the 4DBA layer implies that the π orbitals of the molecules remain practically unsaturated, allowing this system to host foreign atoms and work as a modulating template.

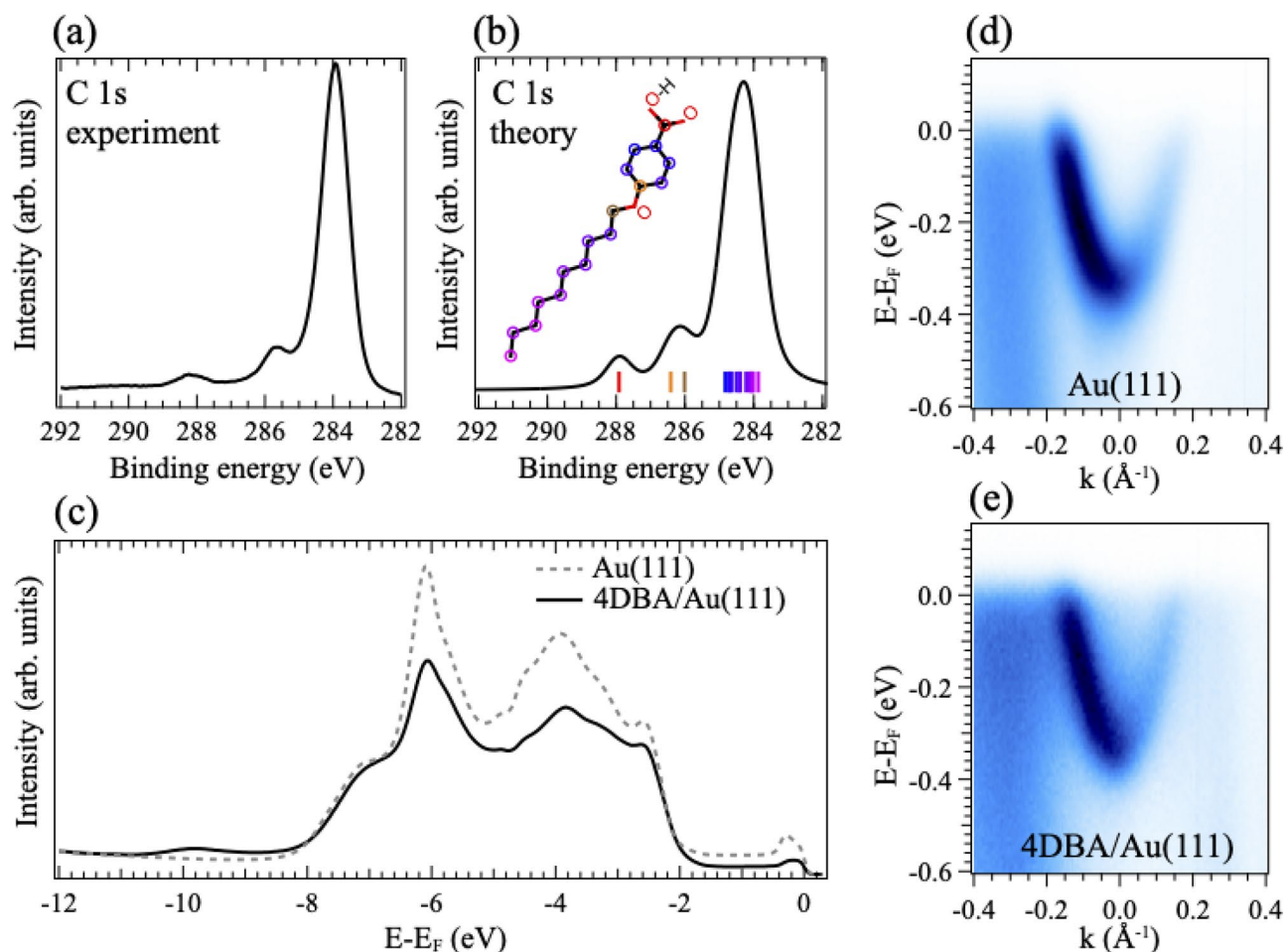


Figure 5. (a) Photoemission spectrum of the C 1s core level region of 4DBA/Au(111) measured at normal emission with photon energy of 350 eV. (b) Simulated C 1s photoemission line for 4DBA in gas phase. The energy positions of the 1s state of the different C atoms are marked by different color bars; A sketch of the 4DBA molecule is shown in the inset. A Voigt shape was adopted for each state. (c) Valence band for bare Au(111) (dotted gray curve), and 4DBA/Au(111) (full black curve) measured at normal emission with photon energy of 45 eV. ARPES map displaying the Shockley surface state of (d) Au(111), and (e) 4DBA/Au(111) measured with photon energy of 45 eV.

Methods

STM measurements were performed in ultra-high vacuum (UHV) conditions (base pressure of 5×10^{-10} mbar) with an Aarhus SPM 150 equipped with KolibriSensor from SPECS operated via Nanonis Control system. STM images were acquired at room temperature (RT) in constant-current mode with a W tip cleaned in UHV by repeated cycles of Ar⁺ sputtering. Tunneling current and voltage are labeled I_t and V_b , respectively. STM measurements were collected both at positive and negative bias voltages resulting in similar results. All STM images were processed using the WSxM software⁶².

Core level and valence band spectra were recorded at RT at the VUV-Photoemission beamline of the Elettra synchrotron radiation facility using a Scienta R4000 electron energy analyzer with a total energy resolution of 30 meV and an angular resolution of 0.1°.

The Au(111) surface (Phasis, a 200 nm of thick Au(111) layer on mica, 99.99% purity), was cleaned by several cycles of Ar⁺ sputtering ($E = 1$ keV for 20 min) followed by annealing ($T = 700$ K for 20 min). The cleanliness quality of the pristine gold surface was verified with STM or photoemission measurements. 4DBA molecules were deposited at RT on Au(111) by organic molecular beam deposition at a pressure of 3×10^{-9} mbar using a home-built evaporator. The evaporation temperature was ~ 345 K. Single-layers of molecules were obtained by ~ 10 sec exposure. A 30 times longer exposure time did not result in multi-layers formation. Annealing the 4DBA/Au at temperatures up to 330 K did not alter the molecular pattern or induced a phase transitions. Annealing at higher temperatures resulted in desorption of the 4DBA molecules.

The electronic structure of both 4DBA conformers were first studied in gas phase using the Quantum Chemistry package Gaussian09⁶³. We carried out a full relaxation of all the coordinates, using an unrestricted double-zeta Pople's 6-31+G(d,p) basis⁶⁴⁻⁶⁷ and the B3LYP functional⁶⁸, without imposing any condition on the symmetry of

Molecule	Phase transitions (°C)
4-HBA	Cr 73 Cr' 106 N 152 I heating
	I 151 N 95 Cr'94 Cr cooling
4-DBA	Cr 88 Cr' 98 Sm 125 N 144 I heating
	I 141 N 123 Sm 94 Cr'76 Cr cooling
4-TBA	Cr 83 Sm 129 I heating
	I 128 N 126 Sm 85 Cr'79 Cr cooling

Table 1. Phase transitions temperatures for the synthesized alkoxy-benzoic acid, Cr, Cr' = crystal phases, Sm = smectic, N = nematic, I = isotropic liquid.

the molecules. These results on the electron structure calculations were also employed to simulate the C 1s and O 1s spectral line shapes.

The molecule self-assembly calculations were carried out using density functional theory within the projector augmented wave (PAW) approach⁶⁹, as implemented in the VASP code^{70–72}, using the Perdew-Burke-Ernzerhof (PBE) exchange correlation functional⁷³ and the Tkatchenko-Scheffler⁷⁴ corrections, to account for weak dispersion forces. Five different types of periodic self-assemblies were taken into account, containing either two or six 4DBA molecules in the 2D unit cell, using a vacuum region of at least 20 Å in the out-of-plane direction. We adopted a 400 eV plane wave cut-off and a total energy threshold of 10^{-5} eV for the self-consistent field calculations. The reciprocal space sampling was carried out using unshifted $6 \times 2 \times 1$ ($3 \times 2 \times 1$ for the six-4DBA molecule per unit cell case), Γ -centered Monkhorst-Pack grids. For each case, several initial conditions (at least three) were tested and the final geometries were obtained relaxing the coordinates of all the atoms until the maximum force was less than 0.01 eV/Å.

The synthesis of the 4-alkoxy-benzoic acid derivatives was performed consistently with the already reported literature^{75,76} through the appropriate modifications reported in Supporting Information (Fig. S5). All three compounds are thermotropic liquid crystals and their thermal behavior was analyzed by differential scanning calorimetry (DSC) and the textures of the mesophases were observed under polarized optical microscope (POM) equipped with a heating stage. Thermotropic behavior of alkoxybenzoic acids is well known and is attributed to the formation of dimers through the carboxylic head-group. The DSC curves and POM micrographs are reported in Supporting Information (Figs. S6–S9). All compounds display polymorphism in their solid state, most likely attributable to a change of conformation of the alkyl chains in the solid state. While 4HBA presents only a nematic mesophase, the longest alkyl chain lengths alkoxybenzoic acids (4DBA and 4TBA) display both smectic and nematic mesophases. However, the temperature range of the monotropic nematic phase displayed by 4TBA is rather reduced (127–129 °C) but well distinguishable due to the observation of a characteristic fingerprint texture displayed on slow cooling from the isotropic temperature (129 °C), just before entering into its smectic mesophase at 127 °C (see Supporting Information for relative POM micrographs). The observation for (alkoxy)benzoic acids of this fingerprint texture, which is usually observed for cholesteric liquid crystals (Chiral nematics) has been postulated to be due to the a chiral-like behaviour of opened dimers. This chiral-like behavior disappears upon further cooling with the concomitant closure of the dimers⁷⁷. The organization of the mesophases for all three compounds are reported in Table 1, and are consistent with results obtained from reported analogues of different or similar alkyl chain lengths^{77,78}.

Data availability

The data that support the findings of this study are available from the corresponding authors upon request.

Received: 18 December 2022; Accepted: 25 January 2023

Published online: 05 February 2023

References

- Lehn, J.-M. Toward self-organization and complex matter. *Science* **295**, 2400–2403. <https://doi.org/10.1126/science.1071063> (2002).
- Barth, J., Weckesser, J., Lin, N., Dmitriev, A. & Kern, K. Supramolecular architectures and nanostructures at metal surfaces. *Appl. Phys. A* **76**, 645–652. <https://doi.org/10.1007/s00339-002-2003-6> (2003).
- Barth, J. V., Costantini, G. & Kern, K. Engineering atomic and molecular nanostructures at surfaces. *Nature* **437**, 671–679. <https://doi.org/10.1038/nature04166>
- Whitesides, G. M. & Grzybowski, B. Self-assembly at all scales. *Science* **295**, 2418–2421. <https://doi.org/10.1126/science.1070821> (2002).
- Zhu, X.-Y. *et al.* Self-assemblies of ttf derivatives programmed by alkyl chains and functional groups. *Phys. Chem. Chem. Phys.* **20**, 6383–6389. <https://doi.org/10.1039/C7CP08201K> (2018).
- Li, J. *et al.* Advances in self-assembly and regulation of aromatic carboxylic acid derivatives at hopg interface. *Chin. Chem. Lett.* **31**, 10–18. <https://doi.org/10.1016/j.ccl.2019.04.032> (2020).
- Weckesser, J., De Vita, A., Barth, J. V., Cai, C. & Kern, K. Mesoscopic correlation of supramolecular chirality in one-dimensional hydrogen-bonded assemblies. *Phys. Rev. Lett.* **87**, 096101. <https://doi.org/10.1103/PhysRevLett.87.096101> (2001).
- Barth, J. V. *et al.* Stereochemical effects in supramolecular self-assembly at surfaces: 1-d versus 2-d enantiomorphic ordering for pvba and peba on ag(111). *J. Am. Chem. Soc.* **124**, 7991–8000. <https://doi.org/10.1021/ja0256764> (2002).
- Smith, R. K., Lewis, P. A. & Weiss, P. S. Patterning self-assembled monolayers. *Prog. Surf. Sci.* **75**, 1–68. <https://doi.org/10.1016/j.progsurf.2003.12.001> (2004).

10. Stepanow, S. *et al.* Steering molecular organization and host guest interactions using two-dimensional nanoporous coordination systems. *Nat. Mater.* **3**, 229–233. <https://doi.org/10.1038/nmat1088> (2004).
11. Rabe, J. P. & Buchholz, S. Commensurability and mobility in two-dimensional molecular patterns on graphite. *Science* **253**, 424–427. <https://doi.org/10.1126/science.253.5018.424> (1991).
12. Philip, D. Supramolecular chemistry: Concepts and perspectives. by j.-m. lehn, vch, weinheim 1995, x, 271 pp., softcover, dm 58.00, isbn 3-527-2931 1-6. *Adv. Mater.* **8**, 866–868. <https://doi.org/10.1002/adma.19960081029> (1996).
13. MacLeod, J. Design and construction of on-surface molecular nanoarchitectures: lessons and trends from trimesic acid and other small carboxylated building blocks. *J. Phys. D Appl. Phys.* **53**, 043002. <https://doi.org/10.1088/1361-6463/ab4c4d> (2019).
14. Bétard, A. & Fischer, R. A. Metal-organic framework thin films: From fundamentals to applications. *Chem. Rev.* **112**, 1055–1083. <https://doi.org/10.1021/cr200167v> (2012) (PMID: 21928861).
15. Heinke, L., Tu, M., Wannapaiboon, S., Fischer, R. A. & Wöll, C. Surface-mounted metal-organic frameworks for applications in sensing and separation. *Microp. Mesop. Mater.* **216**, 200–215. <https://doi.org/10.1016/j.micromeso.2015.03.018> (2015). Special Issue: New Generations of Porous Metal-Organic Frameworks.
16. Ishikawa, Y., Ohira, A., Sakata, M., Hirayama, C. & Kunitake, M. A two-dimensional molecular network structure of trimesic acid prepared by adsorption-induced self-organization. *Chem. Commun.* 2652–2653. <https://doi.org/10.1039/B207556C> (2002).
17. Nath, K. G. *et al.* Rational modulation of the periodicity in linear hydrogen-bonded assemblies of trimesic acid on surfaces. *J. Am. Chem. Soc.* **128**, 4212–4213. <https://doi.org/10.1021/ja0602896> (2006) (PMID: 16568980).
18. Ruben, M. *et al.* 2d supramolecular assemblies of benzene-1,3,5-triyl-tribenzoic acid: Temperature-induced phase transformations and hierarchical organization with macrocyclic molecules. *J. Am. Chem. Soc.* **128**, 15644–15651. <https://doi.org/10.1021/ja063601k> (2006) (PMID: 17147373).
19. Nath, K. G. *et al.* Crystal engineering in two dimensions: An approach to molecular nanopatterning. *J. Phys. Chem. C* **111**, 16996–17007. <https://doi.org/10.1021/jp0762774> (2007).
20. Li, Z. & Wandlowski, T. Structure formation and annealing of isophthalic acid at the electrochemical au(111)-electrolyte interface. *J. Phys. Chem. C* **113**, 7821–7825. <https://doi.org/10.1021/jp900279n> (2009).
21. Mali, K. S., Lava, K., Binnemans, K. & De Feyter, S. Hydrogen bonding versus van der waals interactions: Competitive influence of noncovalent interactions on 2d self-assembly at the liquid solid interface. *Chem. A Eur. J.* **16**, 14447–14458. <https://doi.org/10.1002/chem.201001653> (2010).
22. Cebula, I., Lu, H., Zharnikov, M. & Buck, M. Monolayers of trimesic and isophthalic acid on cu and ag: The influence of coordination strength on adsorption geometry. *Chem. Sci.* **4**, 4455–4464. <https://doi.org/10.1039/C3SC52137K> (2013).
23. Li, J., Gottardi, S., Solianyk, L., Moreno-López, J. C. & Stöhr, M. 1,3,5-benzenetribenzoic acid on cu(111) and graphene/cu(111): A comparative stm study. *J. Phys. Chem. C* **120**, 18093–18098. <https://doi.org/10.1021/acs.jpcc.6b05541> (2016) (PMID: 27588158).
24. Azzam, W. *et al.* Annealing effect for self-assembled monolayers formed from terphenylethanethiol on au(111). *Phys. Chem. Chem. Phys.* **22**, 13580–13591. <https://doi.org/10.1039/D0CP02374D> (2020).
25. Rabot, C., Clair, S., Kim, Y. & Kawai, M. Scanning tunneling microscopy observations of benzoic acid molecules coadsorbed with single-walled carbon nanotubes on au(111) surface. *Jpn. J. Appl. Phys.* **46**, 5572–5576. <https://doi.org/10.1143/jjap.46.5572> (2007).
26. Vu, T.-H. & Wandlowski, T. Cv and in situ stm study the adsorption behavior of benzoic acid at the electrified au(100)|hclo4 interface: Structure and dynamics. *J. Electroanal. Chem.* **776**, 40–48. <https://doi.org/10.1016/j.jelechem.2016.06.039> (2016).
27. Vu, T.-H. & Wandlowski, T. Self-assembled structures of benzoic acid on au (111) surface. *J. Electron. Mater.* **46**, 3463–3471 (2017).
28. nucleation on-command using buffer layers. R., R., Mali, K. S. & De Feyter, S. Growth of a self-assembled monolayer decoupled from the substrate. *Beilstein J. Nanotechnol.* **11**, 1291–1302. <https://doi.org/10.3762/bjnano.11.113> (2020).
29. Hibino, M., Sumi, A., Tsuchiya, H. & Hattai, I. Microscopic origin of the odd even effect in monolayer of fatty acids formed on a graphite surface by scanning tunneling microscopy. *J. Phys. Chem. B* **102**, 4544–4547. <https://doi.org/10.1021/jp973412b> (1998).
30. Baxter, R. J., Teobaldi, G. & Zerbetto, F. Modeling the adsorption of alkanes on an au(111) surface. *Langmuir* **19**, 7335–7340. <https://doi.org/10.1021/la034773n> (2003).
31. Wintgens, D., Yablou, D. G. & Flynn, G. W. Packing of ho(ch₂)₁₄cooh and ho(ch₂)₁₅cooh on graphite at the liquid-solid interface observed by scanning tunneling microscopy: Methylene unit direction of self-assembly structures. *J. Phys. Chem. B* **107**, 173–179. <https://doi.org/10.1021/jp020676b> (2003).
32. HaiMing, Z., Zhao-Xiong, X., Bing-Wei, M. & Xs, X. Self-assembly of normal alkanes on the au (111) surfaces. *Chem. Eur. J.* **10**, 1415–1422. <https://doi.org/10.1002/chem.200305334> (2004).
33. Berner, S. *et al.* Time evolution analysis of a 2d solid-gas equilibrium: A model system for molecular adsorption and diffusion. *Chem. Phys. Lett.* **348**, 175–181. [https://doi.org/10.1016/S0009-2614\(01\)01158-7](https://doi.org/10.1016/S0009-2614(01)01158-7) (2001).
34. Stranick, S. J., Kamna, M. M. & Weiss, P. S. Atomic-scale dynamics of a two-dimensional gas-solid interface. *Science* **266**, 99–102. <https://doi.org/10.1126/science.266.5182.99> (1994).
35. Bürgi, L., Brune, H. & Kern, K. Imaging of electron potential landscapes on au(111). *Phys. Rev. Lett.* **89**, 176801. <https://doi.org/10.1103/PhysRevLett.89.176801> (2002).
36. Barth, J. V., Brune, H., Ertl, G. & Behm, R. J. Scanning tunneling microscopy observations on the reconstructed au(111) surface: Atomic structure, long-range superstructure, rotational domains, and surface defects. *Phys. Rev. B* **42**, 9307–9318. <https://doi.org/10.1103/PhysRevB.42.9307> (1990).
37. De Luca, O. *et al.* Adsorption of Nile red self-assembled monolayers on au(111). *Langmuir* **35**, 14761–14768. <https://doi.org/10.1021/acs.langmuir.9b02416> (2019).
38. De Luca, O. *et al.* Zinc(II) tetraphenylporphyrin on au(111) investigated by scanning tunnelling microscopy and photoemission spectroscopy measurements. *Nanotechnology* **31**, 365603. <https://doi.org/10.1088/1361-6528/ab95ba> (2020).
39. Goronzy, D. P. *et al.* Supramolecular assemblies on surfaces: Nanopatterning, functionality, and reactivity. *ACS Nano* **12**, 7445–7481 (2018). <https://doi.org/10.1021/acsnano.8b0351>.
40. Kühnle, A. Self-assembly of organic molecules at metal surfaces. *Curr. Opin. Colloid Interface Sci.* **14**, 157–168. <https://doi.org/10.1016/j.cocis.2008.01.001> (2009).
41. Maksymovych, P., Sorescu, D. C. & Yates, J. T. Gold-atom-mediated bonding in self-assembled short-chain alkanethiolate species on the au(111) surface. *Phys. Rev. Lett.* **97**, 146103. <https://doi.org/10.1103/PhysRevLett.97.146103> (2006).
42. Yu, M. *et al.* True nature of an archetypal self-assembly system: mobile au-thiolate species on au(111). *Phys. Rev. Lett.* **97**, 166102. <https://doi.org/10.1103/PhysRevLett.97.166102> (2006).
43. Mazzarello, R. *et al.* Structure of a ch₃S monolayer on au(111) solved by the interplay between molecular dynamics calculations and diffraction measurements. *Phys. Rev. Lett.* **98**, 016102. <https://doi.org/10.1103/PhysRevLett.98.016102> (2007).
44. <https://www.ccdc.cam.ac.uk/structures/search?id=https://doi.org/10.5517/ccp76hl1> & sid=DataCite.
45. Su, G.-J., Zhang, H.-M., Wan, L.-J., Bai, C.-L. & Wandlowski, T. Potential-induced phase transition of trimesic acid adlayer on au(111). *J. Phys. Chem. B* **108**, 1931–1937. <https://doi.org/10.1021/jp035095g> (2004).
46. Munakata, T. Dispersion of an adsorption-induced electronic state of benzene/cu(111). *J. Chem. Phys.* **110**, 2736–2737. <https://doi.org/10.1063/1.477999> (1999).
47. Koel, B. E., Crowell, J. E., Mate, C. M. & Somorjai, G. A. A high-resolution electron energy loss spectroscopy study of the surface structure of benzene adsorbed on the rhodium(111) crystal face. *J. Phys. Chem.* **88**, 1988–1996. <https://doi.org/10.1021/j150654a014> (1984).

48. Munakata, T., Sakashita, T., Tsukakoshi, M. & Nakamura, J. Fine structure of the two-photon photoemission from benzene adsorbed on cu(111). *Chem. Phys. Lett.* **271**, 377–380. [https://doi.org/10.1016/S0009-2614\(97\)00458-2](https://doi.org/10.1016/S0009-2614(97)00458-2) (1997).
49. Waddill, G. D. & Kesmodel, L. L. Benzene chemisorption on palladium surfaces. i. high-resolution electron-energy-loss vibrational spectra and structural models. *Phys. Rev. B* **31**, 4940–4946. <https://doi.org/10.1103/PhysRevB.31.4940> (1985).
50. Syomin, D., Kim, J., Koel, B. E. & Ellison, G. B. Identification of adsorbed phenyl (c6h5) groups on metal surfaces: electron-induced dissociation of benzene on au(111). *J. Phys. Chem. B* **105**, 8387–8394. <https://doi.org/10.1021/jp012069e> (2001).
51. Veljković, D., Janjić, G. V. & Zarić, S. D. Are c-h ··· interactions linear? the case of aromatic ch donors. *Cryst. Eng. Comm.* **13**, 5005–5010. <https://doi.org/10.1039/C1CE05065F> (2011).
52. Schwalbe, C. H. June sutor and the c-h ··· hydrogen bonding controversy. *Crystallogr. Rev.* **18**, 191–206. <https://doi.org/10.1080/0889311X.2012.674945> (2012).
53. Stevens, J. S. et al. Incisive probing of intermolecular interactions in molecular crystals: Core level spectroscopy combined with density functional theory. *J. Phys. Chem. B* **118**, 12121–12129. <https://doi.org/10.1021/jp506983s> (2014).
54. Abad, E., Ortega, J., Dappe, Y. J. & Flores, F. Dipoles and band alignment for benzene/au(111) and c 60 /au(111) interfaces (article). *Appl. Phys. A* **95**, 119–124. <https://doi.org/10.1007/s00339-008-5010-4> (2009).
55. Vázquez, H., Dappe, Y. J., Ortega, J. & Flores, F. Energy level alignment at metal/organic semiconductor interfaces: Pillow effect, induced density of interface states, and charge neutrality level. *J. Chem. Phys.* **126**, 144703. <https://doi.org/10.1063/1.2717165> (2007).
56. LaShell, S., McDougall, B. A. & Jensen, E. Spin splitting of an au(111) surface state band observed with angle resolved photoelectron spectroscopy. *Phys. Rev. Lett.* **77**, 3419–3422. <https://doi.org/10.1103/PhysRevLett.77.3419> (1996).
57. Nicolay, G., Reinert, F., Hüfner, S. & Blaha, P. Spin-orbit splitting of the l-gap surface state on au(111) and ag(111). *Phys. Rev. B* **65**, 033407. <https://doi.org/10.1103/PhysRevB.65.033407> (2001).
58. Hövel, H., Grimm, B. & Reihl, B. Modification of the shockley-type surface state on ag (1 1 1) by an adsorbed xenon layer. *Surf. Sci.* **477**, 43–49 (2001).
59. Lindgren, S. Å. & Walldén, L. Photoemission of electrons at the cu(111)/na interface. *Solid State Commun.* **34**, 671–673. [https://doi.org/10.1016/0038-1098\(80\)90952-7](https://doi.org/10.1016/0038-1098(80)90952-7) (1980).
60. Lindgren, S. Å. & Walldén, L. Discrete valence-electron states in thin metal overlayers on a metal. *Phys. Rev. Lett.* **59**, 3003–3006. <https://doi.org/10.1103/PhysRevLett.59.3003> (1987).
61. Pang, W. et al. Epitaxial growth of honeycomb-like stanene on au(111). *Appl. Surf. Sci.* **517**, 146224. <https://doi.org/10.1016/j.apsusc.2020.146224> (2020).
62. Horcas, I. et al. Wsxn: A software for scanning probe microscopy and a tool for nanotechnology. *Rev. Sci. Instrum.* **78**, 013705. <https://doi.org/10.1063/1.2432410> (2007).
63. M. J. Firsich et al. Gaussian 09 Revision E.01 (2013). Gaussian Inc. Wallingford CT.
64. Ditchfield, R., Hehre, W. J. & Pople, J. A. Self consistent molecular orbital methods. ix. an extended gaussian type basis for molecular orbital studies of organic molecules. *J. Chem. Phys.* **54**, 724–728. <https://doi.org/10.1063/1.1674902> (1971).
65. Hehre, W. J., Ditchfield, R. & Pople, J. A. Self consistent molecular orbital methods. xii. further extensions of gaussian type basis sets for use in molecular orbital studies of organic molecules. *J. Chem. Phys.* **56**, 2257–2261. <https://doi.org/10.1063/1.1677527> (1972).
66. Hariharan, P. C. & Pople, J. A. The influence of polarization functions on molecular orbital hydrogenation energies. *Theor. Chim. Acta* **213–222**. <https://doi.org/10.1007/BF00533485> (1973).
67. Francl, M. M. et al. Self consistent molecular orbital methods. xxiii. a polarization type basis set for second row elements. *J. Chem. Phys.* **77**, 3654–3665. <https://doi.org/10.1063/1.444267> (1982).
68. Lee, C., Yang, W. & Parr, R. G. Development of the colle-salvetti correlation-energy formula into a functional of the electron density. *Phys. Rev. B* **37**, 785–789. <https://doi.org/10.1103/PhysRevB.37.785> (1988).
69. Blöchl, P. E. Projector augmented-wave method. *Phys. Rev. B* **50**, 17953–17979. <https://doi.org/10.1103/PhysRevB.50.17953> (1994).
70. Kresse, G. & Joubert, D. From ultrasoft pseudopotentials to the projector augmented-wave method. *Phys. Rev. B* **59**, 1758–1775. <https://doi.org/10.1103/PhysRevB.59.1758> (1999).
71. Kresse, G. & Furthmüller, J. Efficiency of ab-initio total energy calculations for metals and semiconductors using a plane-wave basis set. *Comput. Mater. Sci.* **6**, 15–50. [https://doi.org/10.1016/0927-0256\(96\)00008-0](https://doi.org/10.1016/0927-0256(96)00008-0) (1996).
72. Kresse, G. & Furthmüller, J. Efficient iterative schemes for ab initio total-energy calculations using a plane-wave basis set. *Phys. Rev. B* **54**, 11169–11186. <https://doi.org/10.1103/PhysRevB.54.11169> (1996).
73. Perdew, J. P., Burke, K. & Ernzerhof, M. Generalized gradient approximation made simple. *Phys. Rev. Lett.* **77**, 3865–3868. <https://doi.org/10.1103/PhysRevLett.77.3865> (1996).
74. Tkatchenko, A. & Scheffler, M. Accurate molecular van der waals interactions from ground-state electron density and free-atom reference data. *Phys. Rev. Lett.* **102**, 073005. <https://doi.org/10.1103/PhysRevLett.102.073005> (2009).
75. Ionescu, A. et al. Photoconductive nile red cyclopalladated metallomesogens. *J. Mater. Chem.* **22**, 23617–23626. <https://doi.org/10.1039/C2JM34946A> (2012).
76. Godbert, N. et al. Uv/vis to nir photoconduction in cyclopalladated complexes. *Chem. Asian J.* **4**, 1141–1146. <https://doi.org/10.1002/asia.200900023> (2009).
77. Sparavigna, A. C. Transition bars and related honeycomb and fingerprint textures exhibited by 12OBAC, 16OBAC and a binary mixture of them. *Mech. Mater. Sci. Eng. J.* **12**, 1–9. <https://doi.org/10.2412/mmse.56.32.234> (2017).
78. Jensen, J., Grundy, S. C., Bretz, S. L. & Hartley, C. S. Synthesis and characterization of self-assembled liquid crystals: p-alkoxybenzoic acids. *J. Chem. Educ.* **88**, 1133–1136. <https://doi.org/10.1021/ed101090t> (2011).

Acknowledgements

This work was financially supported by “Progetto STAR2 - PIR0_00008” - Ministero dell’Università e Ricerca/ Italian Ministry of University and Research and by the Advanced Materials research program of the Zernike National Research Centre under the Bonus Incentive Scheme of Ministry for Education, Culture and Science (The Netherlands). The authors acknowledge Elettra Sincrotrone Trieste for providing access to its synchrotron radiation facilities and for financial support. FM acknowledges financial support from the MICINN projects PID2019-105458RB-I00, “Severo Ochoa” Programme for Centers of Excellence in R & D (CEX2020-001039-S), and “Maria de Maeztu” Programme for Units of Excellence in RD (CEX2018-000805-M). MPi and FM acknowledge the generous allocation of computer time by the Red Española de Supercomputación (RES) at the Mare Nostrum computer center and by the Centro de Computación Científica at the Universidad Autónoma de Madrid (CCC-UAM). P.M. acknowledges the project EUROFEL-ROADMAP ESFRI of the Italian Ministry of Education, University, and Research.

Author contributions

T.C. and N.M. performed the scanning tunnelling microscopy measurements. A.P. and P.M. helped with the photoemission experiments. O.D.L. performed the scanning tunnelling microscopy and photoemission measurements and analyzed the data. N.G, M.Pi and F.M. performed the calculations. I.A and E.G. prepared and characterized the molecules. D.P and P.R. provided scientific advice and contributed to the interpretation of the data. R.G.A conceived and planned the project. M.P performed the experiments, analyzed the data and wrote the manuscript with the contribution from all authors.

Competing interests

The authors declare no competing interests.

Additional information

Supplementary Information The online version contains supplementary material available at <https://doi.org/10.1038/s41598-023-28865-w>.

Correspondence and requests for materials should be addressed to M.P.

Reprints and permissions information is available at www.nature.com/reprints.

Publisher's note Springer Nature remains neutral with regard to jurisdictional claims in published maps and institutional affiliations.



Open Access This article is licensed under a Creative Commons Attribution 4.0 International License, which permits use, sharing, adaptation, distribution and reproduction in any medium or format, as long as you give appropriate credit to the original author(s) and the source, provide a link to the Creative Commons licence, and indicate if changes were made. The images or other third party material in this article are included in the article's Creative Commons licence, unless indicated otherwise in a credit line to the material. If material is not included in the article's Creative Commons licence and your intended use is not permitted by statutory regulation or exceeds the permitted use, you will need to obtain permission directly from the copyright holder. To view a copy of this licence, visit <http://creativecommons.org/licenses/by/4.0/>.

© The Author(s) 2023